Journal of Applied Physics

Mechanism leading to semi-insulating property of carbon-doped GaN: Analysis of donor acceptor ratio and method for its determination

Cite as: J. Appl. Phys. **130**, 185702 (2021); https://doi.org/10.1063/5.0060912
Submitted: 23 June 2021 • Accepted: 18 October 2021 • Published Online: 09 November 2021

C. Koller, L. Lymperakis, D. Pogany, et al.

Journal of Applied Physics ARTICLE scitation.org/journal/jap

Mechanism leading to semi-insulating property of carbon-doped GaN: Analysis of donor acceptor ratio and method for its determination

Cite as: J. Appl. Phys. **130**, 185702 (2021); doi: 10.1063/5.0060912
Submitted: 23 June 2021 · Accepted: 18 October 2021 ·
Published Online: 9 November 2021

C. Koller,[1,a)] L. Lymperakis,[2] D. Pogany,[3] G. Pobegen,[1] and C. Ostermaier[4]

AFFILIATIONS

[1]KAI GmbH, Europastraße 8, 9524 Villach, Austria
[2]Max-Planck-Institut für Eisenforschung GmbH, Max-Planck-Straße 1, 40237 Düsseldorf, Germany
[3]Institute of Solid State Electronics, TU Wien, Gußhausstraße 25a, 1040 Vienna, Austria
[4]Infineon Technologies Austria AG, Siemensstraße 2, 9500 Villach, Austria

[a)]**Author to whom correspondence should be addressed:** christian.koller2@k-ai.at

ABSTRACT

Carbon impurities in GaN form both acceptors and donors. Donor-to-acceptor ratios (DARs) determine the semi-insulating behavior of carbon-doped GaN (GaN:C) layers and are still debated. Two models are discussed; both can theoretically achieve semi-insulating behavior: the dominant acceptor model (DAM, DAR < 1) and the auto-compensation model (ACM, DAR $= 1$). We perform a capacitance–voltage analysis on metal/GaN:C/nGaN (n-doped GaN) structures, exhibiting Fermi-level pinning in GaN:C, 0.7 eV above the valence band maximum. This observation coupled with further interpretation clearly supports the DAM and contradicts the ACM. Furthermore, we reveal a finite depletion width of a transition region in GaN:C next to nGaN, where carbon acceptors drop below the Fermi level becoming fully ionized. Calculation of the potential drop in this region exhibits DAR values of 0.5–0.67 for GaN:C with total carbon concentrations of 10^{18} cm^{-3} and 10^{19} cm^{-3}. Based on those results, we re-evaluate formerly published density functional theory (DFT)-calculated formation energies of point defects in GaN. Unexpectedly, growth in thermodynamic equilibrium with the bulk carbon phase contradicts our experimental analysis. Therefore, we propose the consideration of extreme carbon-rich growth conditions. As bulk carbon and carbon cluster formation are not reported to date, we consider a metastable GaN:C solid solution with the competing carbon bulk phase being kinetically hindered. DFT and experimental results agree, confirming the role of carbon at nitrogen sites as dominant acceptors. Under N-rich conditions, carbon at gallium sites is the dominant donor, whereas additional nitrogen vacancies are generated under Ga-rich conditions.

I. INTRODUCTION

GaN-on-Si high-electron-mobility transistors (HEMTs) for power applications require highly insulating GaN buffers.[1] They have to prevent detrimental leakage current between electrically active GaN layers on the top and the electrically inactive Si substrate on the bottom. It is empirically well known that carbon doping makes GaN buffers semi-insulating;[2,3] however, the underlying mechanism is still discussed.

In unintentionally doped GaN, especially if grown on Si substrates, a high number of impurity atoms in the range of 10^{16} cm^{-3} exists. The greatest part of them acts as shallow donors, pushing the Fermi level close to the conduction band. This makes the material n-type and, therefore, rather conductive. In order to compensate these donor impurities, other impurities such as Be,[4] Fe,[5,6] or carbon[2] can be added. In this work and for most power applications, carbon is used. The key of these impurities is to push the Fermi level away from the band edges, making the material semi-insulating. Depending on the growth conditions of carbon-doped GaN (GaN:C), i.e., Ga-rich vs N-rich, and the position of the Fermi level during growth, carbon atoms can be built in at different lattice sites, which can act as either acceptors or donors.[7] Most relevant are carbon atoms on gallium sites (C_{Ga}), which act as donors with concentration N_d and on nitrogen sites (C_N), acting as acceptors with concentration N_a. Consequently, the carbon concentration N_C is the sum of N_d and N_a. Density-functional-theory (DFT)-based simulations[7–9] suggest that the donor level is shallow,

close to the conduction band minimum, whereby its exact energy E_d is unknown. For C_N acceptors, DFT simulations and optical[7–9] and electrical characterization by deep level transient spectroscopy (DLTS)-like methods[10–13] suggest energy levels E_a in the range of 0.5–1.1 eV above the valence band maximum (E_V). However, the trapping behavior in GaN might be limited by the transport process through GaN rather than the capture and emission properties of carbon defects,[13–16] making DLTS-like analysis rather questionable for extraction of defect energy levels.[14]

For modeling the electrical properties of GaN:C, knowledge of the total carbon concentration is not sufficient; it is important to know the defect parameters, in particular, the donor-to-acceptor ratio, DAR = N_d/N_a. DAR determines the relative position of the Fermi level within the bandgap,[17] which has consequences to the electrical behavior, such as the leakage current,[18] dynamic on-resistance,[19] and their modeling.[13]

In literature, one distinguishes between two models of Fermi-level pinning in relation to DAR: the *auto-compensation model* (ACM) with DAR = 1 and the *dominant acceptor model* (DAM) with DAR < 1.[8,16,20,21] For ACM shown in Fig. 1(a), the Fermi level is located in the center between the donor energy level E_d and the acceptor energy level E_a. Figure 1(b) demonstrates that in DAM the Fermi level is pinned close to E_a.

DFT simulations[7,8] suggest that the dominant site for carbon incorporation depends on the growth conditions; this consequently determines the form of the pinning mechanism. The ACM is expected under N-rich growth where C_N and C_{Ga} are favorable under n-type and p-type conditions, respectively. However, under Ga-rich growth, C_N is energetically favorable for Fermi levels (E_F) above $E_V + \approx 0.6$ eV with a transition level of $E_V + \approx 0.9$ eV. Hence, the DAM is anticipated under these growth conditions. Interestingly, electrical characterization could not confirm this clear distinction. For example, for MOCVD-grown GaN:C, which are the most relevant for industrial applications, both models have been reported.[20,22]

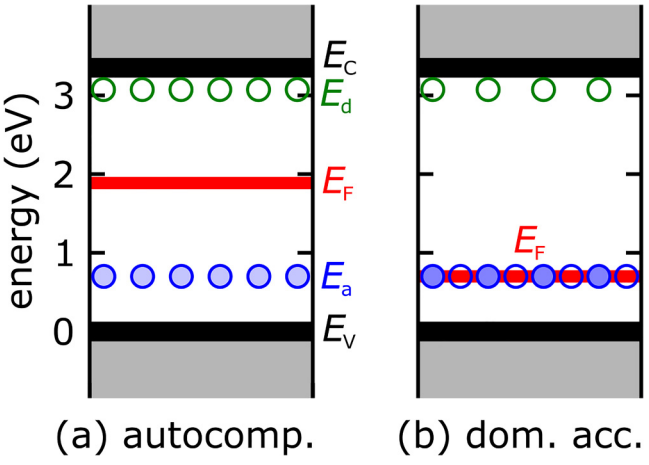

FIG. 1. Band diagrams with the calculated Fermi level, considering the (a) ACM and the (b) DAM, with E_a = 0.7 eV, E_d= 3.1 eV, and DAR of 0.5 in (b). Carbon dopant concentrations play no role. Empty circles represent unoccupied dopants, whereas filled circles represent occupied dopants.

In short, there is no consensus about the DAR value, the Fermi level pinning mechanism, and how the semi-insulating behavior in GaN:C is achieved. We have recently shown by capacitance–voltage (C-V) characterization of metal/GaN:C/n-doped GaN (nGaN) structures with $N_C = 10^{19}$ cm^{-3} that the Fermi level in GaN is pinned at E_V + 0.7 eV. This supports the DAM[23] though no DAR has been determined in this study. Furthermore, based on the analysis of suppression of two-dimensional hole gas in AlGaN/AlN/GaN:C structures, Rackauskas *et al.* estimated DARs in GaN:C in the range of 0.4–1.0, which also support the DAM.[22]

In our present work, we provide further support in favor of the DAM and present an enhanced C–V analysis method for determination of DAR using metal/GaN:C/nGaN structures. In Sec. II, a detailed analysis of Fermi-level pinning on defect parameters for the ACM and the DAM is performed and supporting arguments in favor of the DAM are summarized. In Sec. III, the method for DAR determination is presented. It is based on considering the finite width of a negatively charged transition region in GaN:C close to the GaN:C/nGaN interface in the analysis of C–V data. Characterization of samples with carbon concentrations lower than those used previously[23] allows for DAR extraction with a better accuracy than in previous works.[22]

Furthermore, in Sec. IV, we examine DFT calculated formation energies[7,8] of various defects. Common GaN devices with insulating GaN buffers exhibit carbon concentrations as high as 10^{19} cm^{-3}. However, we demonstrate that this can only be achieved if extreme carbon-rich and metastable growth conditions are considered. Furthermore, despite MOCVD growth with expected N-rich conditions, electrically observed Fermi-level pinning levels and DAR values suggest rather Ga-rich growth. In Sec. IV, we discuss these discrepancies and provide a different perspective that can explain a higher carbon concentration while having the Fermi level pinned below E_V + 1 eV.

II. AUTO-COMPENSATION VS DOMINANT ACCEPTOR MODEL

In this section, we discuss whether the semi-insulating behavior of GaN:C is due to the ACM or the DAM. Therefore, we interpret the result of our previous publication[23] that analyzed the aforementioned test structures and conclude that the Fermi level pins stably at $E_V + (0.7 \pm 0.2)$ eV. In the following, we describe three features of GaN:C with respect to its pinned Fermi level that excludes the possibility of the ACM and leaves only the DAM as the reason for the semi-insulating behavior of GaN:C. The features are (A) the value of the pinned Fermi level in equilibrium, (B) discussion of the stability of the Fermi level under small acceptor and donor concentration fluctuations, and (C) the analysis of the Fermi level after charge trapping.

A. Fermi-level pinning at E_V + 0.7 eV

In the following, we consider E_F in GaN:C at E_V + 0.7 eV[23] and calculate the possible configurations of E_a and E_d levels to keep E_F constant. We consider the charge neutrality equation within GaN:C for flatband conditions, i.e., sufficiently far from its

interfaces,

$$n(E_F, T) + N_a^-(E_F, T, E_a, \mu_{Ga}, \mu_C) + N^* = p(E_F, T) + N_d^+(E_F, T, E_d, \mu_{Ga}, \mu_C), \quad (1)$$

with μ_{Ga} and μ_C being respective chemical potentials of Ga and C atoms, which will be discussed in Sec. IV in more detail. N^* is an additional space charge density as discussed in Sec. II C. If not explicitly specified, it is considered 0. The electron concentration n and hole concentration p in addition to the concentrations of ionized acceptors N_a^- (negatively charged, occupied) and donors N_d^+ (positively charged, unoccupied) depend on the temperature T and E_F. They can be expressed as

$$\begin{aligned} n(E_F, T) &= N_{CB}(T) \exp\left(-\frac{E_C - E_F}{k_B T}\right), \\ N_a^-(E_F, T, E_a) &= N_a f_{FDD}[E_a - E_F, T], \\ p(E_F, T) &= N_{VB}(T) \exp\left(-\frac{E_F - E_V}{k_B T}\right), \\ N_d^+(E_F, T, E_d) &= N_d\,(1 - f_{FDD}[E_F - E_d, T]), \end{aligned} \quad (2)$$

with the effective density of states in the conduction band N_{CB} and valence band N_{VB}, and the Fermi–Dirac distribution function f_{FDD}. The position of E_F is uniquely defined by the charge neutrality condition in (1). Thus, E_F depends on temperature T, the donor energy levels E_d, and acceptor energy levels E_a as well as growth conditions, i.e., values of μ_{Ga} and μ_C.

In the following, we assume that charge neutrality pins the Fermi level at E_V + 0.7 eV and we deduce the donor and acceptor levels that allow us to achieve an (a) ACM with DAR = 1 and a (b) DAM with DAR = 0.5. The corresponding band diagrams are plotted in Figs. 2(a) and 2(b). Figure 2(a) illustrates that the pinning of E_F at E_V + 0.7 eV can be achieved by various configurations of E_d and E_a: for demonstrative purposes, we sweep the value of E_d and calculate E_a using (1) so that the value of E_F becomes constant. In the ACM [Fig. 2(a)], E_F lies directly at the central position ($(E_d + E_a)/2$). For values of $E_d - E_F$ between 0 and 0.7 eV (i.e., E_d between E_V + 0.7 eV and E_V + 1.4 eV), E_F pins exactly between E_a and E_d. However, as E_a is shifted closer to E_V, E_d is located slightly nearer to E_F. In this region, the acceptor level is shallow, and hence, the concentration of free holes increases and has a sizeable effect on E_F pinning.

On the other hand, Fig. 2(b) demonstrates that in the DAM, even if E_d is greatly varied from roughly E_V + 0.75 eV to E_C while E_a is kept constant at E_V + 0.7 eV, E_F keeps pinning at E_V + 0.7 eV. The reason is that as long as E_d is few tens of above E_F, it is practically fully ionized and the ionization rate shows negligible change with increasing E_d.

One may ask whether the activation energy of the carbon acceptor decreases with increasing carbon concentration and whether it can influence our conclusions. Therefore, we have performed Fermi-level calculations as in Fig. 2 but for an exaggeratedly low E_a level at E_V + 0.4 eV. The results are however insensitive to the exact value of E_a and show nearly the same DAR values as for the used $E_a = E_V + 0.7$ eV. Same applies for higher E_a values, e.g., $E_a = E_V + 1.1$ eV.

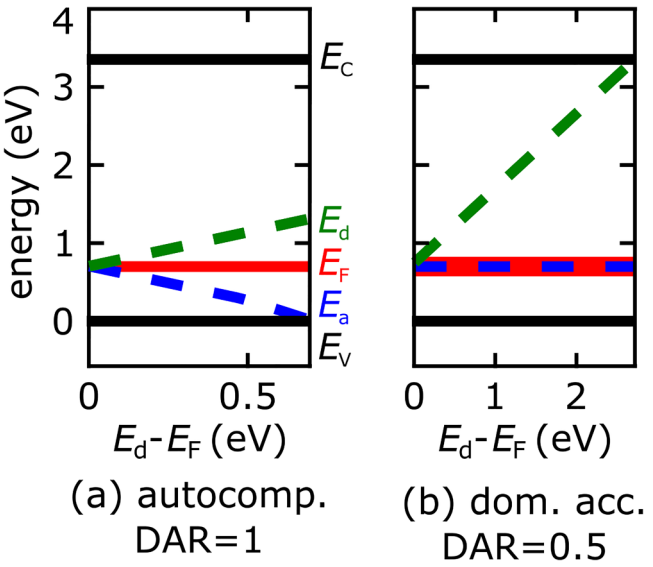

FIG. 2. On the basis of (1), calculated sets of E_a and E_d that establish the experimentally derived Fermi level at E_V + 0.7 eV, considering $N_C = 10^{19}\text{cm}^{-3}$ and an (a) ACM with DAR = 1 and a (b) DAM with DAR = 0.5. From left to right, E_d is increased and E_a adjusted so that E_F stays at E_V + 0.7 eV.

As introduced above, E_a is expected in the range of 0.5–1.1 eV above E_V,[7–13] while E_d is reported close to the conduction band.[7–9] Figure 2 reveals that this configuration is only possible considering the DAM.

B. Acceptor and donor concentration fluctuations

We have performed electrical characterization on samples with varying growth conditions that lead to carbon concentrations of N_C = [1,10,70] × 10^{18}cm^{-3}.[23,24] We would expect that with varying carbon concentrations, DAR should fluctuate to some extent. Remarkably, we emphasize that the extracted position of E_F at approximately E_V + 0.7 eV is a general feature and independent of the carbon concentration within the investigated range.[23,24]

Using (1), we investigate E_F as a function of DAR for the ACM in Fig. 3(a) and the DAM in Fig. 3(b), considering fixed values of E_a and E_d. It is clear that for the ACM, a sub-percent deviation from DAR = 1 results in a significant shift in E_F [Fig. 3(a)]. This clearly contradicts our experimental observations of a stable Fermi level. Instead of the DAM in (b), given a wide range of DAR roughly between 0.01 and 0.99, the Fermi level is stable in the vicinity of E_a. Even significant changes in DAR do not lead to significantly different electrical behavior, fitting to experimental results.

C. Fermi level after charge trapping

Electrical characterization in Refs. 23 and 24 reveals that even after significant negative charge trapping, the Fermi level within the GaN:C bulk is still pinned at E_V + 0.7 eV. Also in commercially

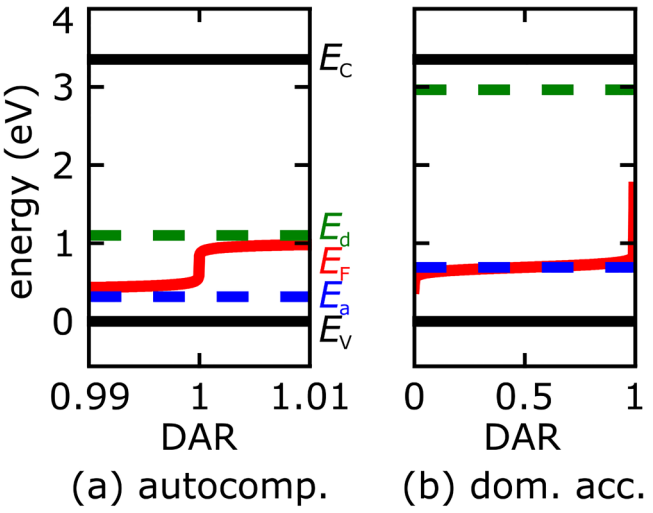

FIG. 3. On the basis of (1), the calculated Fermi level considering $N_C = 10^{19}\text{cm}^{-3}$ for an (a) ACM with $E_a = E_V + 0.3$ eV and $E_d = E_V + 1.1$ eV as well as a (b) DAM with $E_a = E_V + 0.7$ eV and $E_d = E_V + 3$ eV. From left to right, DAR increases.

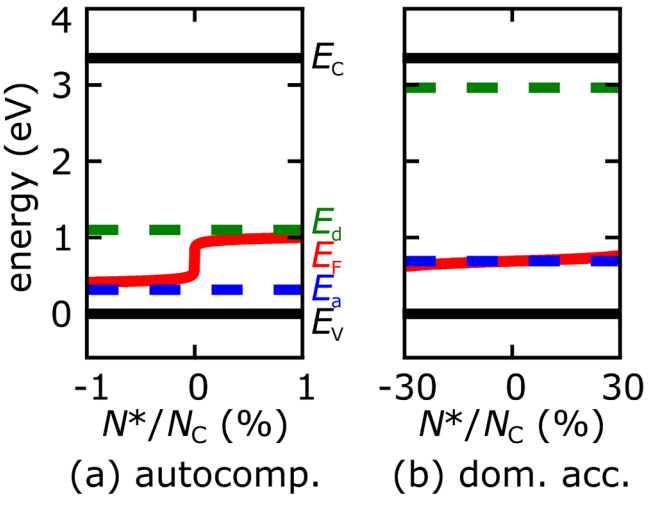

FIG. 4. On the basis of (1), the calculated Fermi level considering $N_C = 10^{19}\text{cm}^{-3}$ and an (a) ACM with DAR = 1 and a (b) DAM with DAR = 0.5. In order to reflect the change of the Fermi level, an additional space charge density of N^* (e.g., after charge trapping) is used in (1).

available GaN HEMTs with carbon-doped buffers, significant amounts of electrons up to several $10^{12}\,\text{cm}^{-2}$ are trapped in the buffer.[25] As this does not change the semi-insulating behavior of GaN:C, we consider that the Fermi level does not shift significantly by the capture of electrons.

Figure 4 shows the Fermi level for the (a) ACM and the (b) DAM considering a certain density of trapped charges per volume N^*. For the calculation, (1) is used with the additional charge density N^* on the left side of the equation. For example, if applying bias leads to negative charge capture in carbon acceptors, while n and p stay negligible, a positive space charge of $N^* = -N_a^- + N_d^+$ would establish. This case will be discussed in detail in Sec. III. Figure 4(a) reveals that for the ACM, the Fermi level would shift significantly due to trapping, even for densities N^* in the sub-percent range of N_C. For the DAM, the Fermi level is up to roughly ± 30 of N_C pinned in the vicinity of N_a, fitting well to the experimental results.

In conclusion, all three discussed aspects can only be explained properly by the DAM and contradict the ACM. This information is crucial for understanding the relevant parameters for achieving semi-insulating GaN:C and how to optimize the epitaxial growth.

III. METHOD FOR DAR DETERMINATION

After verifying the validity of the dominant acceptor model, we use this knowledge in order to estimate all the relevant defect parameters, E_a, N_a, and N_d, which also allow for the extraction of DAR. Figure 2(b) has revealed that E_d is not relevant. We use simple nGaN/GaN:C bilayers and perform simple capacitance–voltage measurements. These points discussed in the first part of Sec. III A have already been introduced in Refs. 23, 24, and 26 and are only briefly summarized here. The new approach is presented in Sec. III B, which also discusses the nGaN/GaN:C interface in more detail.

A. Test structures and electrical characterization

Figure 5 shows the investigated structures that are based on 6-in. n-doped Si(111) substrates with MOCVD-grown GaN layers on top. All samples consist of a transition layer and a 1.7 μm thick Si-doped GaN layer (nGaN) that acts as an n-type semiconductor with an active donor concentration of $(8.4 \pm 0.2) \times 10^{16}\,\text{cm}^{-3}$.[23] Unlike sample S_{ref}, S_{01} and S_{10} include an additional GaN:C layer on top with a thickness of approximately 200 nm. Secondary ion mass spectroscopy (SIMS) reveals atomistic carbon concentra-tions of 10^{18} cm^{-3} for S_{01} and 10^{19} cm^{-3} for S_{10}. All structures finish with deposited square Ti contacts with an edge length of 100 µm.

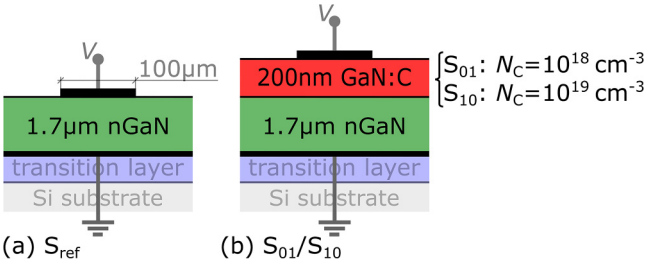

FIG. 5. (a) Reference sample S_{ref} and (b) samples S_{01} and S_{10} including GaN:C layers with carbon concentration N_C as indicated.

The outstanding feature of these test structures is that current is localized in GaN:C solely under the metal contacts and distributed then in the nGaN layer over the entire wafer. Hence the impedance of all layers below nGaN can be neglected which allows for the investigation of a simple nGaN/GaN:C bilayer.

The total small-signal capacitance C of these structures can be expressed as a series of the capacitance (C_{Si}) of the depleted nGaN layer and the constant capacitance of the GaN:C layer (C_C) for samples S_{01} and S_{10},[23]

$$\frac{1}{C} = \frac{1}{C_{Si}} + \frac{1}{C_C}, \qquad C_{Si} = \frac{\varepsilon}{d_{Si}}, \quad C_C = \frac{\varepsilon}{d}, \tag{3}$$

with permittivity ε and the thickness of the GaN:C layer d. Capacitance measurements are performed with a small-signal frequency of 10. Trap relaxation time constants in GaN:C are in the range of 300, i.e., orders of magnitude larger than the reciprocal value of the frequency. Consequently, trapping in GaN:C does not follow the small signal. The voltage ramp for C–V characterization instead is chosen with 30 so that the trap occupancy follows the voltage ramp.

The capacitance of nGaN (C_{Si}) is determined by its depletion width (d_{Si}), which depends on the doping concentration (N_{Si}) and the potential drop in nGaN (V_{Si}),[23]

$$C_{Si} = \sqrt{\frac{q\varepsilon N_{Si}}{2\,V_{Si}}}, \tag{4}$$

$$d_{Si} = \frac{\varepsilon}{C_{Si}}, \tag{5}$$

with q being the elementary charge. V_{Si} in S_{ref} is determined by the applied bias V and V_{bi}, which is the Schottky barrier at the nGaN surface as indicated in Fig. 8(a). In S_{01} and S_{10} with the additional GaN:C layers, V_{bi} is the energy difference between the metal and the conduction band minimum in the GaN:C bulk. Additionally, a potential drop in GaN:C (V_C) has to be considered,

$$\begin{aligned} S_{ref}&: V_{Si} = -V + V_{bi}, \\ S_{01}\text{ and }S_{10}&: V_{Si} = -V + V_{bi} - V_C. \end{aligned} \tag{6}$$

Equations (3)–(6) are the basis for the analysis of electrical characterization of the test structures for reverse bias in Fig. 6. The introduction of V_C in the equations is the novelty with respect to Ref. 23. The I–V curves shown in Fig. 6(a) indicate that the depletion of nGaN prevents major leakage currents. The leakage current is even more suppressed with an additional GaN:C layer on top of nGaN as in S_{01} and S_{10}. Figure 6(c) reveals a vertical offset in $\frac{1}{C} - V$ curves between S_{10} and S_{ref}, which is due to the additional C_C, and follows (3) directly. $\frac{1}{C^2} - V$ in Fig. 6(d) for S_{ref} follows (6) directly and the linear dependence with the same slope from 0 to −35 reveals that the nGaN layer is homogeneously doped with a concentration of approximately $8.4 \times 10^{16}\,\mathrm{cm}^{-3}$. As all three samples are from the same lot, this homogeneity also applies for

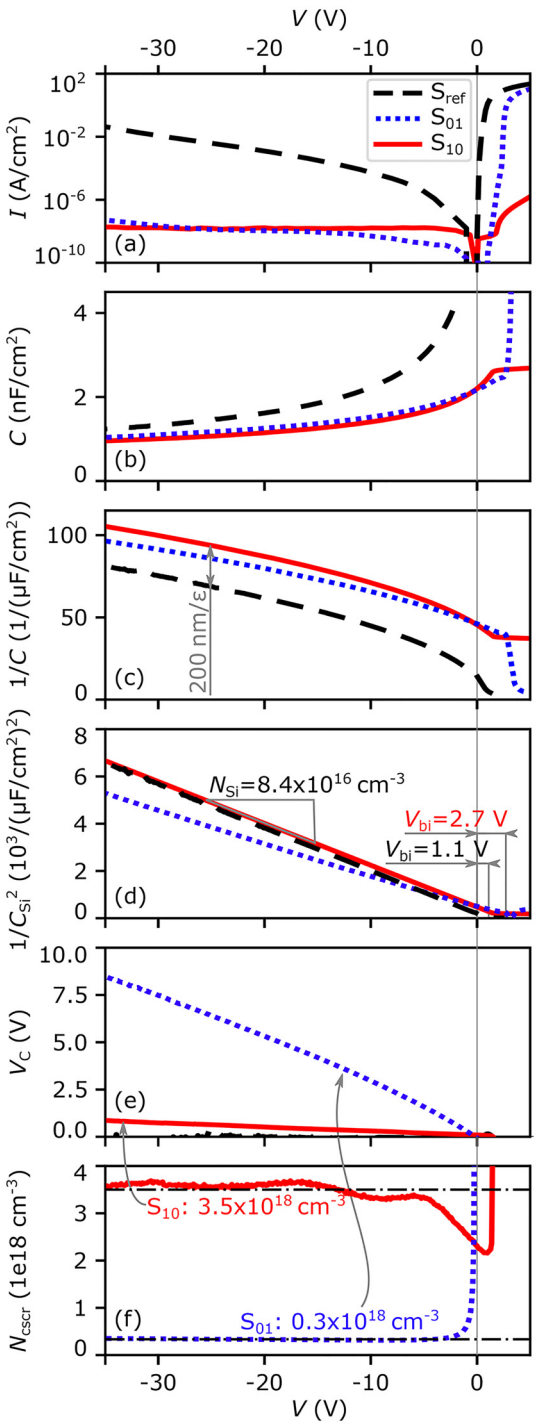

FIG. 6. (a) Current density I vs applied bias V, (b) capacitance density C vs V, (c) $1/C$, (d) $1/C_{Si}^2$ with C_{Si} calculated from (3), (e) the potential drop in GaN:C (V_C) calculated from (9), and (f) the concentration of charge in the carbon space charge region (N_{cscr}) calculated from (8). For the derivation of V_C in (e), the average values for N_{cscr} as indicated in (f) by dashed-dotted lines are used.

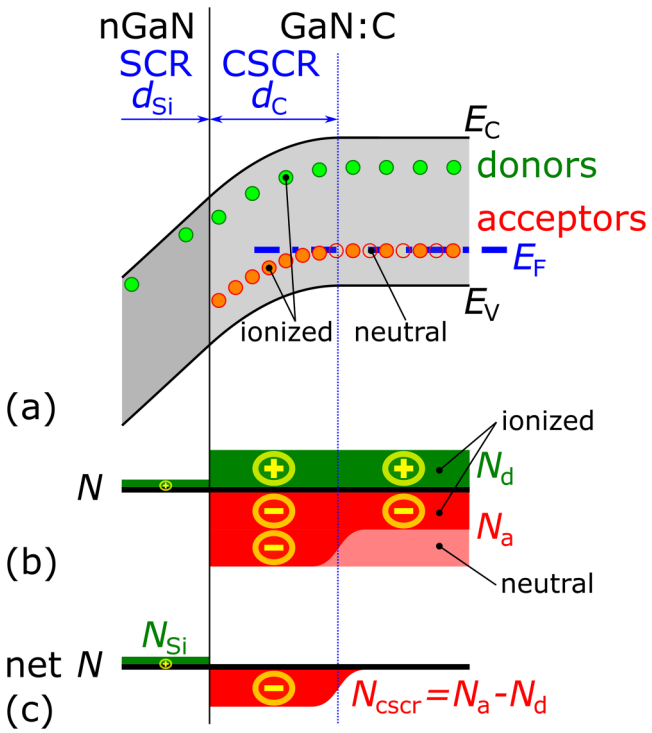

FIG. 7. (a) Schematic band diagram, (b) concentrations of ionized and neutral acceptors and donors, and (c) ("carbon") net densities at the nGaN/GaN:C interface considering DAR = 0.5.

S_{01} and S_{10}. In our previous articles,[14,23,24] V_C has been neglected. A comparison of $\frac{1}{C_{Si}^2} - V$ curves of S_{01} and S_{10} with S_{ref} in Fig. 6(d) reveals little discrepancies for low voltages and for the highly carbon-doped sample S_{10}, making this simplification appropriate. However, more detailed analysis reveals reproducible and significant deviations, especially of S_{01} with increasing negative bias. To understand the origin of this discrepancy and the relation to V_C, Sec. III B discusses the nGaN/GaN:C interface region in detail.

B. Estimations of acceptor and donor concentrations and DAR

In all samples, the positive space charge in the depleted nGaN generates a positive charge per area (σ_{Si}),

$$\sigma_{Si} = q\, N_{Si}\, d_{Si}. \tag{7}$$

While in S_{ref} this charge is compensated in the top metal, in S_{01} and S_{10} negative charge has to accumulate in GaN:C.[23] Figure 7 shows a schematic of the nGaN/GaN:C interface region, which incorporates the knowledge of the aforementioned pinning mechanism. As the relevant interface region is small compared to the nGaN depletion region, only a fraction of nGaN depletion is shown. Due to the small part of the nGaN region being shown, the potential in nGaN appears to decrease linearly, although it changes quadratically with the distance. This becomes clear in Fig. 8(c), which illustrates the band diagram of the entire nGaN/GaN:C junction. Figure 7(a) shows the band diagram, (b) the ionization of defects, and (c) the net density of charges N, which relates to the net space charge densities qN. On the left side, nGaN is depleted, resulting in a space charge region (SCR) with depletion width d_{Si}, which is only partly shown. On the very right side, there is the neutral GaN:C bulk with the identical amount of ionized acceptors and donors, resulting in charge neutrality. The region of interest in this section is the part of GaN:C directly next to nGaN, in which carbon acceptors sink below the Fermi level and get occupied. This results in a net negative charge within a region we refer to as "carbon" space charge region (CSCR) with a "carbon" space charge density ($q\, N_{cscr}$) of maximum $q(N_a\text{-}N_d)$. Our distinction between SCR and CSCR emphasizes that unlike the classical SCR, in the CSCR, the net charge does not rise from depletion of free electrons or holes but by a change of the defect (i.e., carbon acceptor) occupancy.

The CSCR width (d_C) can be calculated from

$$d_C = d_{Si}\,\frac{N_{Si}}{N_{cscr}}. \tag{8}$$

Within this CSCR, the potential decreases with the square of the distance resulting in a total potential drop in GaN:C (V_C) of

$$V_C = \frac{q\, N_{cscr}\, {d_C}^2}{2\varepsilon} = \frac{\sigma_C d_C}{2\varepsilon}, \tag{9}$$

with $\sigma_C = qN_{cscr}d_C$ as equivalent sheet charge density in GaN:C equal to $qN_{Si}d_{Si}$. Equations (8) and (9) show that with increasing N_C and consequently increasing N_{cscr}, both d_C and V_C decrease. Considering $N_C = 10^{19}\,\mathrm{cm}^{-13}$ and neglecting defects besides carbon, DAR of 0.5 is achieved, where $N_a = 6.6\times10^{18}\,\mathrm{cm}^{-13}$, $N_d = 3.3\times10^{18}\,\mathrm{cm}^{-13}$, and consequently $N_{cscr} = 3.3\times10^{18}\,\mathrm{cm}^{-13}$. d_C is then roughly 40 times smaller than d_{Si} and therefore does not exceed a few under any relevant bias conditions. In earlier publications,[14,23,24] we ignored the finite value of d_C and considered the negative charges directly at the nGaN/GaN:C interface. However, with increasing negative bias and decreasing N_C from $10^{19}\,\mathrm{cm}^{-13}$ to $10^{18}\,\mathrm{cm}^{-13}$, the value of d_C is not negligible anymore. This manifests itself in a significant deviation of the $\frac{1}{C_{Si}^2} - V$ curves of S_{01} from the reference sample S_{ref} in Fig. 6(d). We use this deviation and (4) as well as (6) to extract V_C as a function of the bias, as shown in Fig. 6(e). With negative bias, not only d_{Si} but also V_C increases. Using (9), N_{cscr} can be extracted as depicted in Fig. 6(f). In principle, N_{cscr} could be extracted from a single bias point. If the origin for V_C is the potential drop within CSCR, N_{cscr} has to be constant over a wide bias range. As Fig. 6(f) demonstrates, this is the case for both S_{01} and S_{10}.

Using the extracted N_{cscr} values for S_{01} and S_{10}, the potential distributions at the nGaN/GaN:C interface can be calculated for samples S_{01} and S_{10}, see Figs. 8(b) and 8(c). They demonstrate that for sample S_{10} the potential drop in GaN:C (V_C) is insignificant and can be neglected as has been suggested in earlier works.[14,23,24] This does not apply for sample S_{01} in Fig. 8(c), explaining the significant deviations of $\frac{1}{C} - V$ and $\frac{1}{C_{Si}^2} - V$ curves in Figs. 6(c) and 6(d).

Extracted N_{cscr} values in Fig. 6(f) deliver values of 0.3 and $3.5\times10^{18}\,\mathrm{cm}^{-13}$ for samples S_{01} and S_{10}, respectively. We can use

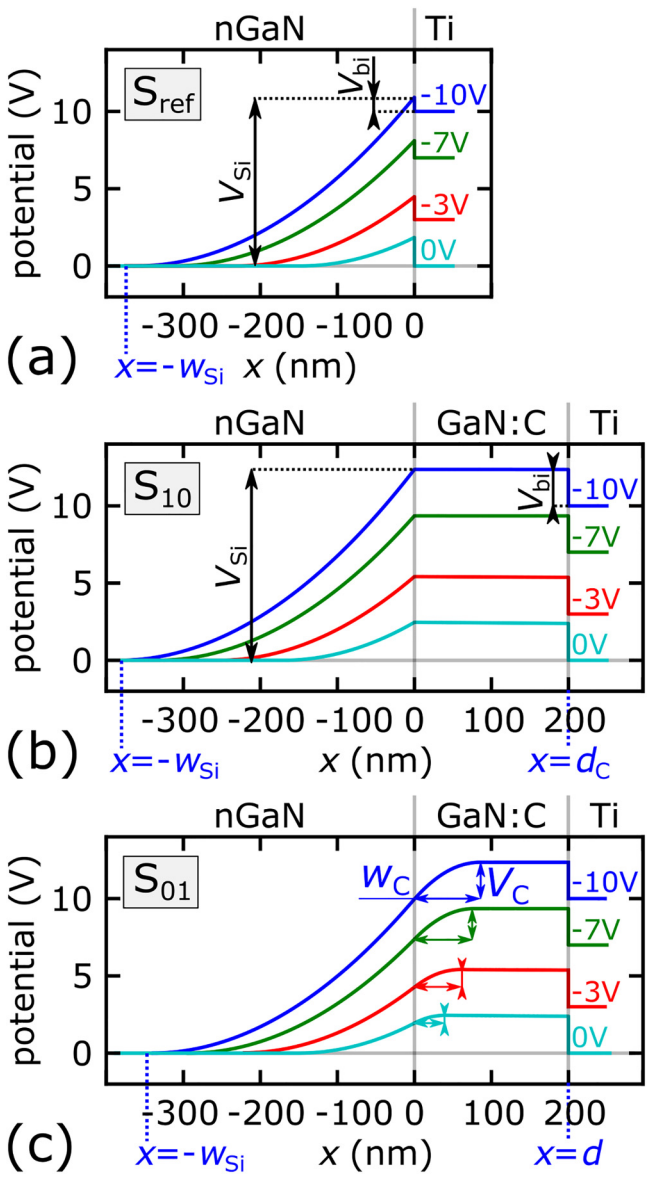

FIG. 8. Calculated band diagrams (conduction band minima) for the samples (a) S_{ref}, (b) S_{10}, and (c) S_{01} based on *CV* data from Fig. 6(b). Due to roughly ten times higher carbon concentration in S_{10} compared to S_{01}, the potential drop V_C and width d_C in GaN:C are almost invisible in (b) but very distinct in (c).

these values to estimate acceptor and donor concentrations as well as corresponding values for DAR. As all impurities apart from carbon typically have concentrations well below 10^{17} cm^{-13}, we can neglect them for first approximation. As discussed in detail in Sec. IV, defects such as nitrogen vacancies V_N, which are not related to impurities and act as donors have to be considered. Consequently, we consider all acceptors originating from carbon, while donors can be related to carbon or to nitrogen vacancies with respective densities of $N_d(C)$ and $N_d(V_N)$ such that $N_d = N_d(C) + N_d(V_N)$. In the following, we consider two scenarios regarding the origin of N_d. (1) For V_N concentrations significantly smaller than the carbon concentration, they can be neglected. Therefore, $N_{cscr} = N_a - N_d(C)$ and $N_C = N_a + N_d(C)$, resulting in $N_a = (N_C + N_{cscr})/2 \approx 0.67 \times N_C$ and $N_d(C) = (N_C - N_{cscr})/2 \approx 0.33 N_C$. This means that approximately 2/3 of carbon atoms form acceptors and 1/3 donors, giving DAR = 0.5. (2) If V_N concentrations are in the range of, or even exceeding the carbon concentration, they are no longer non-negligible. With increasing V_N concentrations, the amount of carbon atoms that form acceptors increases from 67% for negligible V_N concentrations up to 100% for V_N concentrations being equal to N_C. In the latter case, $N_{cscr} = N_a - N_d(V_N)$ and $N_C = N_a$, resulting in $N_a = N_C$ and $N_d(V_N) = N_a - N_{cscr} \approx 0.67 \times N_C$, giving DAR = 0.67. If donors originate from carbon defects and nitrogen vacancies, DAR values are between 0.5 and 0.67. V_N concentrations exceeding the carbon concentration would not result in a DAM and can be excluded. In a recent study,[22] it has been shown that carbon doping can suppress the formation of a two-dimensional hole gas in AlGaN/AlN/AlGaN:C heterostructures. It has been pointed out that this suppression requires DAR in AlGaN:C in the range of 0.4–1.0, fitting well to the derived value in this study.

As shown in Fig. 3(b), DAR = 0.5 results in Fermi-level pinning exactly at E_a. Knowledge of $E_F = E_V + 0.7$ eV also reveals $E_a = E_V + 0.7$ eV. Therefore, this analysis has revealed all aforementioned relevant parameters of the GaN:C defect model (E_a, N_a, and N_d).

In general, the pinning mechanism and especially the exact value of the DAR might depend on the exact growth conditions. However, comparison with results from literature suggest that the observed pinning behavior is not limited to the observed samples but a rather general behavior of highly carbon-doped GaN layers. As mentioned above, Rackauskas *et al.*[27] also evaluated DAR values between 0.4 and 1. Wang *et al.*[28] investigated similar nGaN/GaN:C bilayers and observed comparable electrical characteristics, fitting well to the described DAM but not to ACM. Further discussion on the influence of growth conditions follows in Sec. IV.

Knowledge of the pinning mechanism for achieving insulating behavior in GaN:C and exact DAR values, acceptor and donor concentrations, is crucial for various purposes. If one can monitor the defect parameters properly, the development of the epitaxial growth could change from a "trial and error"-based approach to a more knowledge-based approach. This information aids in understanding electrical buffer-related device features of HEMTs such as the horizontal and vertical leakage current, the dynamic on-resistance, and current collapse. Furthermore, it opens up the possibility to simulate GaN stacks by technology computer-aided design (TCAD) with proper intrinsic defect properties.

IV. DFT-BASED ANALYSIS OF DOPANTS' CONCENTRATIONS, FERMI-LEVEL PINNING, AND DAR

A. Computational approach

In the following, we try to shed light on the experimental findings of C concentrations in the range of 10^{18}–10^{19} cm^{-3} and the Fermi-level pinning mechanism, i.e., DAM and DAR. Therefore, we employ density functional theory (DFT) calculated formation

energies and thermodynamic transition levels of point defects in GaN from literature,[29–31] and we calculate the concentration and position of the Fermi level for various growth conditions. The influence of the surface on C incorporation is not considered. We consider C dopants in GaN, i.e., C substitutionals at Ga and N site (C_{Ga} and C_N) and interstitials (C_i),[29] and native point defects, i.e., Ga and N vacancies, interstitials, and antisites.[30] The presence of extrinsic donors, such as Si (Si_{Ga}) or O (O_N) substitutionals, has not been considered. High concentrations of these impurities may shift the Fermi level higher in the bandgap. However, neither of them are present in the investigated layers. This is confirmed by secondary-ion mass spectroscopy (SIMS) measurements that exclude concentrations of both above the measurement resolution limit of roughly 10^{16} cm^3. Furthermore, H is present in MOCVD growth and hence we also consider H interstitials (H_i)[31] and the complex of a C substitutional at the N site with a H interstitial (C_N-H). We fix the H chemical potential to the value of −1.32 eV, with respect to the chemical potential of H in H_2 molecule. This value corresponds to $T = 965\,^{\circ}$C and partial pressure $p_{H_2} = 25$ mbar, i.e., similar to the experimental growth conditions. Moreover, for the Ga and N chemical potentials, we consider equilibrium with GaN, i.e., $\mu_{Ga} + \mu_N = \mu_{GaN}$. Figure 9 shows the formation energy of the aforementioned defects and the defect complex for Ga-rich conditions ($\Delta\mu_{Ga} = 0$) as a function of the Fermi level.

In thermodynamic equilibrium, the concentration c_X^q of a point defect or a defect complex X at a charge state q is

$$c_X^q(T) = N_{\text{sites}}\, g\, \exp\left(-E_f(X^q)/(k_B T)\right), \tag{10}$$

where N_{sites} is the density of lattice sites where the defect can be incorporated and g is the degeneracy. The formation energy $E_f(X^q)$ is given by

$$E_f(X^q) = \Delta E(X^q) - \sum_i n_i \mu_i + q E_F, \tag{11}$$

where $\Delta E(X^q)$ is the total energy difference between the system with the defect and without. n_i is the number of atoms of species i added ($n_i > 0$) or removed ($n_i < 0$) to create the defect and μ_i is their chemical potential. In the following, we write the chemical potentials of the species with respect to the value in the corresponding chemical reservoir $\mu_{i\,\text{ref}}$, i.e., $\Delta\mu_i = \mu_i - \mu_{i\,\text{ref}}$. These are the orthorombic α-Ga, diamond C, and N_2 and H_2 molecules. The Fermi level in Eq. (11) is referenced to the bulk E_V.

As it is apparent from Eqs. (10) and (11), the formation energy and hence the concentration of each defect depend on the values of the chemical potentials and the position of the Fermi level. The value of the chemical potentials depends on the partial pressure and temperature and can be experimentally controlled.[32] However, the position of the Fermi level, i.e., the electronic chemical potential, is not directly varied. Instead, it is ultimately determined by the condition of charge neutrality [see Eqs. (1) and (2)].

B. Results and discussion

In Fig. 10(a), we employ Eqs. (1), (2), (10), and (11) and calculate the total C concentration N_C (see color code in legend), the ratio of donors over acceptors (DAR, see blue dashed contour lines), and the position of the Fermi level in respect to E_V (black contour lines) as a function of the Ga and C chemical potentials (x and y axes, respectively). The position of the Fermi level for charge neutrality is calculated at room temperature.

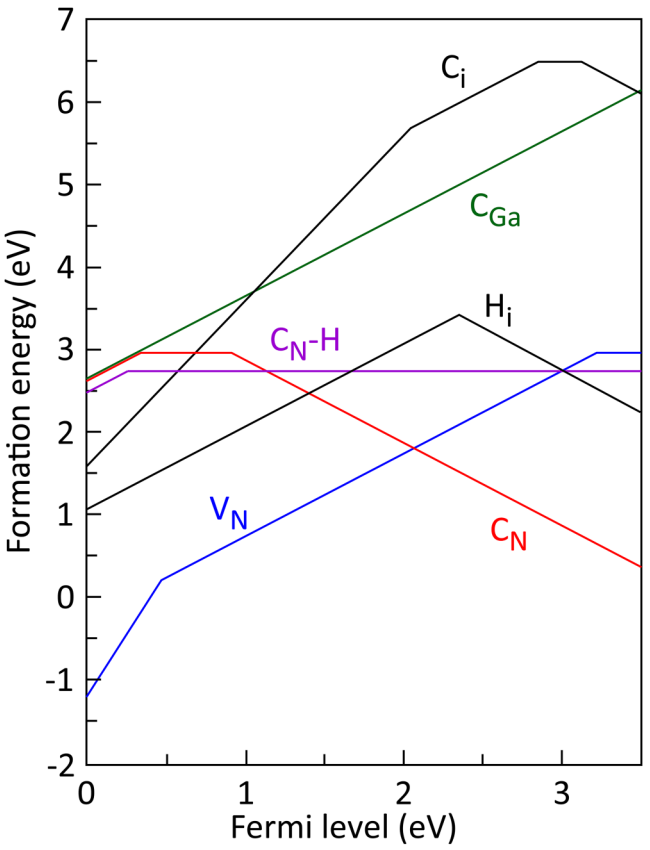

FIG. 9. Formation energy vs Fermi level for substitutional (C_{Ga} and C_N) and interstitial (C_i) C configurations and C_N–H complex in GaN under Ga-rich conditions (i.e., $\Delta\mu_{Ga} = 0$). The formation energy of V_N is plotted for comparison. The formation energies of C_{Ga}, C_N, and C_i and of V_N are from Refs. 29 and 30, respectively. The formation energy of the C_N–H complex has been calculated in the present study employing HSE calculations. The chemical potential of H is fixed at $\Delta\mu_H = -1.32$ eV (see text). Growth under N-rich conditions will rigidly shift the formation energies of C_N, C_N–H, and V_N upward and C_{Ga} downward by ΔH^f, whereby ΔH^f is the absolute value of the GaN formation enthalpy.

A commonly applied approach is to investigate defect concentrations at the thermodynamically allowed extreme values of the chemical potentials, i.e., $\Delta\mu_i = 0$. These are indicated by white stars on the left (for C- and N -rich conditions, i.e., $\Delta\mu_C = 0$ and $\Delta\mu_{Ga} = -\Delta H^f$, where ΔH^f is the formation enthalpy of GaN) and on the right (for C- and Ga-rich conditions, i.e., $\Delta\mu_C = 0$ and $\Delta\mu_{Ga} = 0$) stars in Fig. 10(a). At $\Delta\mu_C = 0$, the Fermi level is pinned at ≈3.15 eV above the bulk E_V. For N-rich conditions, the total C concentration is less than 10^{10} cm^{-3} and for Ga-rich conditions ≈ 3×10^{13} cm^{-3}, while the DAR is ≈ 40 for N-rich and ≈ 2 for Ga-rich conditions.

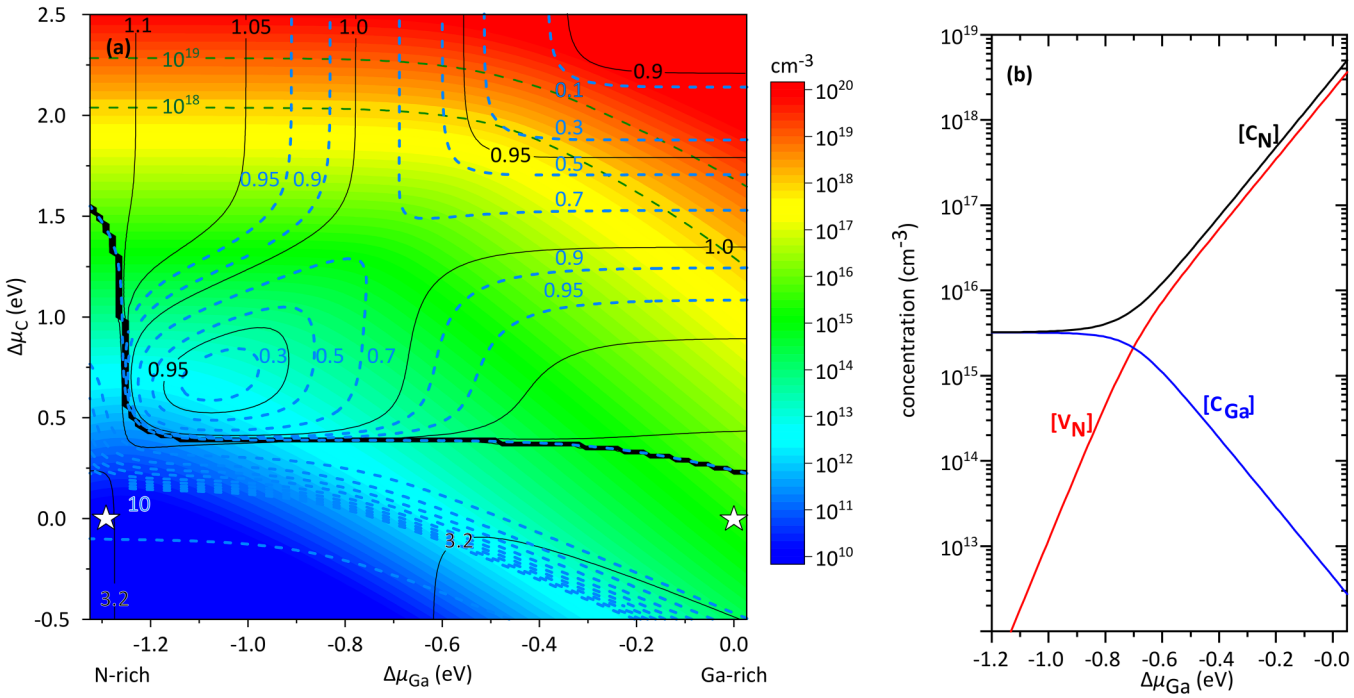

FIG. 10. (a) Total carbon concentration N_C as a function of Ga and C chemical potentials. The green dashed contour lines indicate the experimentally obtained C concentrations, i.e., 10^{18} and 10^{19} cm^{-3}. The black solid contour lines denote the position of the Fermi level for charge neutrality at room temperature in the presence of C dopants and native point defects. The blue dashed contour lines indicate the ratio of donors (i.e., C_{Ga}, C_i, and V_N) over acceptors (i.e., C_N). For positive values of the C chemical potential, i.e., $\Delta\mu_C > 0$, the GaN:C solid solution is in a metastable state. (b) Concentrations of the dominant point defects as a function of the Ga chemical potential for $\Delta\mu_C$ = 1.5 eV: carbon substitutionals at gallium site ([C_{Ga}]), carbon substitutionals at nitrogen site ([C_N]), and nitrogen vacancies ([V_N]).

The above-mentioned findings are in apparent contrast to our electrical measurements and to the experimentally measured C concentrations of 10^{18} cm^{-3} and above. A possible route to achieve high C contents is to compensate C acceptors by an approximately equal number of activated extrinsic donors. However, as already mentioned, possible extrinsic donors such as Si_{Ga} or O_N substitutionals are not present in high concentrations in the investigated layers. In order to address this, in the following, we focus on the energetics of point defects in bulk and we investigate possible routes to achieve high C concentrations. The formation energy can be decreased and the concentration of C dopants can be increased if $\Delta\mu_C$ is raised to positive values.

In this case, the GaN:C solid solution is in principle unstable against separation toward GaN and bulk C. However, according to the best of our knowledge, the formation of C precipitates at the growth of high C content semi-insulating GaN layers has not been reported. Hence, in the present work, we consider that GaN:C is in a metastable state. Figure 11 demonstrates that this can be achieved if surface and/or gas phase kinetics hinder the formation of the competing C bulk phases, i.e., diamond or graphite. The system is then kinetically restricted into a metastable growth regime. Stabilization of metastable phases by kinetics has been reported in III–V semiconductors such as the kinetic stabilization of N contents above the bulk solubility limits in InAs[33] and the surface-induced ordering in InGaN and AlGaN alloys.[34,35]

Figure 10(a) reveals that in order to achieve C contents of 10^{18} cm^{-3} and above, the C chemical potential has to be raised above ≈1.5 eV. The figure also demonstrates that below ≈0.4 eV the Fermi

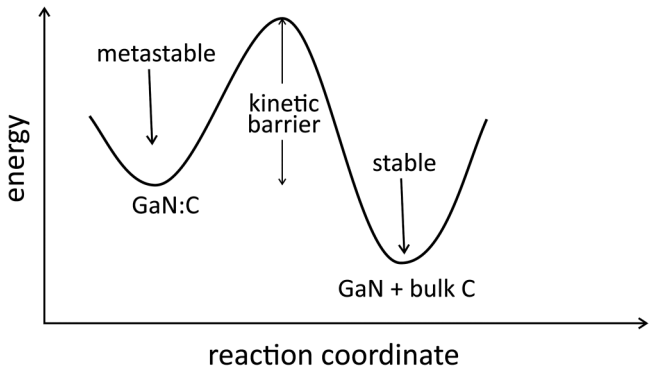

FIG. 11. Schematic representation of the GaN–C system being in a metastable and a stable state. The C chemical potential is raised to a positive value ($\Delta\mu_C > 0$). Therefore, the system is unstable against diamond C. If, however, the formation of a bulk C competing phase is kinetically hindered, a GaN:C solid solution can be stabilized in a metastable state.

level is close to the conduction band (E_F values of 3.1–3.2 eV), which would cause n-type behavior. This changes rapidly above this threshold of ≈0.4 eV where the Fermi level starts to pin close to E_a (E_F values of 0.95–1.1 eV). This is also well seen by the thick black line in Fig. 10(a) which is a crowding of contour lines for values between 1.1 and 3.0 eV. For high $\Delta\mu_C$ values and N-rich growth, DAR values are very close to 1, indicating ACM. However, this is again contrary to the electrical properties of semi-insulating behavior of GaN:C as discussed earlier. In order to achieve experimentally observed DAR values in the range of 0.5–0.7, the Ga chemical potential has to be above roughly −0.7 eV. We notice that there is also a region with DAR values significantly below 1 for rather N-rich conditions and $\Delta\mu_C \approx 0.4$–1.2 eV. However, this results in carbon concentrations lower than 10^{16} cm^{-3}, for which earlier neglected impurities such as Si and O might become relevant and dominate the electrical characteristics, preventing semi-insulating behavior.

MOCVD and MOVPE of III-nitrides are performed under high V/III input ratios and as a result are commonly considered to take place under N-rich conditions. Nevertheless, the near equilibrium conditions at the vapor–solid interface that determine the stable and/or metastable bulk phases may be considerably different from those in the input gas phase. These conditions have a strong dependence on and are a complex interplay between the diffusion and chemical kinetics in the gas phase and on the surface.[36,37] A direct quantitative correlation of the growth conditions, i.e., partial pressures of precursors and growth temperature, with $\Delta\mu_i$ is beyond the scope of the present article. Nevertheless, previous *in situ* ellipsometry measurements on MOVPE growth of InGaN alloys revealed the presence of excess metal on the surface despite the high V/III input ratio.[38] The latter is a strong indication that the corresponding Ga chemical potential is far from the thermodynamically allowed limit of N-rich conditions. Moreover, a comparison of a DFT calculated surface phase diagram with surface reconstruction transitions revealed by *in situ* grazing incidence x-ray scattering on GaN(0001) surfaces in an MOCVD environment indicated that the presence of excess metal corresponds to transitions that appear in the phase diagram at $\Delta\mu_{Ga} \gtrsim -0.7$ eV.[39,40] This is far from the calculated thermodynamically allowed N-rich limit ($\Delta\mu_{Ga} \approx -1.25$ eV), supporting our assumption of Ga-rich growth conditions despite high V/III input ratios.

Within the aforementioned growth window, i.e., $\Delta\mu_C > 1.5$ eV and $\Delta\mu_{Ga} > -0.7$ eV, the DAR decreases with the C chemical potential and reveals values similar to the ones observed by electrical measurements, i.e., 0.5–0.67, for $\Delta\mu_C \approx +1.6$ eV [see Fig. 10(a)]. Therefore, highly insulating carbon-doped GaN with the observed pinning mechanism can be achieved as metastable GaN:C solid solution under moderate Ga-rich to Ga-rich and extremely C-rich, i.e., $\Delta\mu_C > 0$, conditions. In Fig. 10(b), the concentrations of the dominant point defects at $\Delta\mu_C = +1.5$ eV, i.e., C_N, C_{Ga}, and V_N, are plotted against the Ga chemical potential. For $\Delta\mu_{Ga} > -0.7$ eV, V_N are the dominant donor species and C_N are the dominant acceptor species.

V. CONCLUSION

We analyzed formerly reported mechanisms that can lead to Fermi-level pinning in GaN:C and make it semi-insulating. On the basis of three features of the pinned Fermi level in GaN:C within nGaN/GaN:C bilayers, we can exclude the auto-compensation model (ACM), i.e., the same amount of acceptors and donors, as the origin for the semi-insulating behavior of GaN:C. Instead, a dominant acceptor model (DAM) in combination with a minor donor pins the Fermi level approximately 0.7 eV above the valence band maximum. We introduced a detailed analysis method to derive the potential drop in GaN:C next to nGaN, which allows quantitative extraction of the acceptor and donor concentrations. The experiments suggest that for two samples with carbon concentrations N_C of 10^{18} cm^{-13} and 10^{19} cm^{-13}, more than 2/3 of carbon atoms form acceptors. These acceptors are partly compensated by donors, originating from carbon donors or nitrogen vacancies with a total donor concentration between 1/3 and 2/3 of N_C. This results in donor-to-acceptor ratios (DARs) between 0.5 and 0.67, respectively. The analysis in this work is able to provide all relevant defect parameters (E_a, N_a, and N_d). This helps, for example, to generate an intrinsic GaN:C model for TCAD.

Evaluation of prior DFT calculations on point defects in bulk GaN show that high C content in the range of 10^{18}–10^{19} cm^{-3} with the Fermi level pinned below E_V+1 eV can be achieved only under extreme C-rich conditions, i.e., $\Delta\mu_C > 0$. Growth under these conditions requires that the competing bulk phase of C is kinetically hindered and the GaN:C solid solution is in a metastable state. Although kinetic stabilization of high C contents at the surface at lower values of $\Delta\mu_C$ is beyond the scope of the present study and cannot be excluded, the aforementioned analysis is in agreement with the experimental finding that the dominant acceptor mechanism governs Fermi-level pinning. The Fermi level is pinned close to the acceptors' energy level with C_N being the the dominant acceptor species and V_V being the dominant donors.

ACKNOWLEDGMENTS

The authors thank M. Uren for valuable discussion and motivation to publish. C. Koller, G. Pobegen, and D. Pogany have received funding from the Austrian Research Promotion Agency (FFG, Project No. 881110). Furthermore, C. Ostermaier and L. Lymperakis received funding from the ECSEL Joint Undertaking (JU) under Grant Agreement No. 826392. The JU receives support from the European Union's Horizon 2020 research and innovation programme and Austria, Belgium, Germany, Italy, Slovakia, Spain, Sweden, Norway, and Switzerland.

AUTHOR DECLARATIONS

Conflict of Interest

The authors have no conflicts to disclose.

DATA AVAILABILITY

The data that support the findings of this study are available from the corresponding author upon reasonable request.

REFERENCES

[1]K. J. Chen, O. Häberlen, A. Lidow, C. L. Tsai, T. Ueda, Y. Uemoto, and Y. Wu, "GaN-on-Si power technology: Devices and applications," IEEE Trans. Electron Devices **64**, 779–795 (2017).

[2]J. B. Webb, H. Tang, S. Rolfe, and J. A. Bardwell, "Semi-insulating C-doped GaN and high-mobility AlGaN/GaN heterostructures grown by ammonia molecular beam epitaxy," Appl. Phys. Lett. **75**, 953–955 (1999).
[3]M. Huber, I. Daumiller, A. Andreev, M. Silvestri, L. Knuuttila, A. Lundskog, M. Wahl, M. Kopnarski, and A. Bonanni, "Characterization of AlN/AlGaN/GaN:C heterostructures grown on Si(111) using atom probe tomography, secondary ion mass spectrometry, and vertical current-voltage measurements," J. Appl. Phys. **119**, 125701 (2016).
[4]H. Ahmad, T. J. Anderson, J. C. Gallagher, E. A. Clinton, Z. Engel, C. M. Matthews, and W. Alan Doolittle, "Beryllium doped semi-insulating GaN without surface accumulation for homoepitaxial high power devices," J. Appl. Phys. **127**, 215703 (2020).
[5]S. Heikman, S. Keller, S. P. DenBaars, and U. K. Mishra, "Growth of Fe doped semi-insulating GaN by metalorganic chemical vapor deposition," Appl. Phys. Lett. **81**, 439–441 (2002).
[6]M. Kubota, T. Onuma, Y. Ishihara, A. Usui, A. Uedono, and S. F. Chichibu, "Thermal stability of semi-insulating property of Fe-doped GaN bulk films studied by photoluminescence and monoenergetic positron annihilation techniques," J. Appl. Phys. **105**, 083542 (2009).
[7]J. L. Lyons, A. Janotti, and C. G. V. de Walle, "Carbon impurities and the yellow luminescence in GaN," Appl. Phys. Lett. **97**, 152108 (2010).
[8]A. F. Wright, "Substitutional and interstitial carbon in wurtzite GaN," J. Appl. Phys. **92**, 2575–2585 (2002).
[9]C. H. Seager, A. F. Wright, J. Yu, and W. Götz, "Role of carbon in GaN," J. Appl. Phys. **92**, 6553–6560 (2002).
[10]C. Zhou, Q. Jiang, S. Huang, and K. J. Chen, "Vertical leakage/breakdown mechanisms in AlGaN/GaN-on-Si devices," IEEE Electron Device Lett. **33**, 1132–1134 (2012).
[11]A. Chini, G. Meneghesso, M. Meneghini, F. Fantini, G. Verzellesi, A. Patti, and F. Iucolano, "Experimental and numerical analysis of hole emission process from carbon-related traps in GaN buffer layers," IEEE Trans. Electron Devices **63**, 3473–3478 (2016).
[12]D. Bisi, M. Meneghini, C. De Santi, A. Chini, M. Dammann, P. Bruckner, M. Mikulla, G. Meneghesso, and E. Zanoni, "Deep-level characterization in GaN HEMTs-part I: Advantages and limitations of drain current transient measurements," IEEE Trans. Electron Devices **60**, 3166–3175 (2013).
[13]M. Uren, S. Karboyan, I. Chatterjee, A. Pooth, P. Moens, A. Banerjee, and M. Kuball, "'Leaky dielectric' model for the suppression of dynamic Ron in carbon-doped AlGaN/GaN HEMTs," in *IEEE Transactions on Electron Devices* (IEEE, 2017), pp. 1–9.
[14]C. Koller, G. Pobegen, C. Ostermaier, and D. Pogany, "Evidence of defect band in carbon-doped GaN controlling leakage current and trapping dynamics," in *2017 IEEE International Electron Devices Meeting (IEDM)* (IEEE, 2017), pp. 33.4.1—33.4.4.
[15]M. Singh, M. J. Uren, T. Martin, S. Karboyan, H. Chandrasekar, and M. Kuball, "'Kink' in AlGaN/GaN-HEMTs: Floating buffer model," IEEE Trans. Electron Devices **65**, 3746–3753 (2018).
[16]A. Armstrong, C. Poblenz, D. S. Green, U. K. Mishra, J. S. Speck, and S. A. Ringel, "Impact of substrate temperature on the incorporation of carbon-related defects and mechanism for semi-insulating behavior in GaN grown by molecular beam epitaxy," Appl. Phys. Lett. **88**, 082114 (2006).
[17]R. A. Smith, *Semiconductors* (Cambridge University Press, 1978).
[18]C. Poblenz, P. Waltereit, S. Rajan, S. Heikman, U. K. Mishra, and J. S. Speck, "Effect of carbon doping on buffer leakage in AlGaN/GaN high electron mobility transistors," J. Vac. Sci. Technol. B **22**, 1145–1149 (2004).
[19]G. Meneghesso, M. Meneghini, and E. Zanoni, *Gallium Nitride-Enabled High Frequency and High Efficiency Power Conversion* (Springer, 2018).
[20]G. Verzellesi, L. Morassi, G. Meneghesso, M. Meneghini, E. Zanoni, G. Pozzovivo, S. Lavanga, T. Detzel, O. Häberlen, and G. Curatola, "Influence of buffer carbon doping on pulse and ac behavior of insulated-gate field-plated power AlGaN/GaN HEMTs," IEEE Electron Device Lett. **35**, 443–445 (2014).
[21]G. Curatola and G. Verzellesi, "Modelling of GaN HEMTs: From device-level simulation to virtual prototyping," in *Power GaN Devices: Materials, Applications and Reliability*, edited by M. Meneghini, G. Meneghesso, and E. Zanoni (Springer International Publishing, Cham, 2017), pp. 165–196.
[22]B. Rackauskas, M. J. Uren, S. Stoffels, M. Zhao, S. Decoutere, and M. Kuball, "Determination of the self-compensation ratio of carbon in AlGaN for HEMTs," IEEE Trans. Electron Devices **65**, 1838–1842 (2018).
[23]C. Koller, G. Pobegen, C. Ostermaier, M. Huber, and D. Pogany, "The interplay of blocking properties with charge and potential redistribution in thin carbon-doped GaN on n-doped GaN layers," Appl. Phys. Lett. **111**, 032106 (2017).
[24]C. Koller, G. Pobegen, C. Ostermaier, and D. Pogany, "Effect of carbon doping on charging/discharging dynamics and leakage behavior of carbon-doped GaN," IEEE Trans. Electron Devices **65**, 5314–5321 (2018).
[25]M. J. Uren and M. Kuball, "Impact of carbon in the buffer on power switching GaN-on-Si and RF GaN-on-SiC HEMTs," Jpn. J. Appl. Phys. **60**, SB0802 (2021).
[26]C. Koller, G. Pobegen, C. Ostermaier, G. Hecke, R. Neumann, M. Holzbauer, G. Strasser, and D. Pogany, "Trap-related breakdown and filamentary conduction in carbon doped GaN," Phys. Status Solidi B **256**, 1800527 (2019).
[27]B. Rackauskas, S. Dalcanale, M. J. Uren, T. Kachi, and M. Kuball, "Leakage mechanisms in GaN-on-GaN vertical pn diodes," Appl. Phys. Lett. **112**, 233501 (2018).
[28]J. Wang, H. You, H. Guo, J. Xue, G. Yang, D. Chen, B. Liu, H. Lu, R. Zhang, and Y. Zheng, "Do all screw dislocations cause leakage in GaN-based devices?," Appl. Phys. Lett. **116**, 062104 (2020).
[29]J. L. Lyons, A. Janotti, and C. G. Van de Walle, "Effects of carbon on the electrical and optical properties of InN, GaN, and AlN," Phys. Rev. B **89**, 035204 (2014).
[30]J. L. Lyons and C. G. V. de Walle, Comput. Mater. **3**, 12 (2017).
[31]C. G. Van de Walle and J. Neugebauer, "Universal alignment of hydrogen levels in semiconductors, insulators and solutions," Nature **423**, 626–628 (2003).
[32]A. I. Duff, L. Lymperakis, and J. Neugebauer, "*Ab initio*-based bulk and surface thermodynamics of InGaN alloys: Investigating the effects of strain and surface polarity," Phys. Status Solidi B **252**, 855–865 (2015).
[33]H. Abu-Farsakh and J. Neugebauer, "Enhancing nitrogen solubility in GaAs and InAs by surface kinetics: An *ab initio* study," Phys. Rev. B **79**, 155311 (2009).
[34]L. Lymperakis, T. Schulz, C. Freysoldt, M. Anikeeva, Z. Chen, X. Zheng, B. Shen, C. Chèze, M. Siekacz, X. Q. Wang, M. Albrecht, and J. Neugebauer, "Elastically frustrated rehybridization: Origin of chemical order and compositional limits in InGaN quantum wells," Phys. Rev. Mater. **2**, 011601 (2018).
[35]M. Albrecht, L. Lymperakis, J. Neugebauer, J. E. Northrup, L. Kirste, M. Leroux, I. Grzegory, S. Porowski, and H. P. Strunk, "Chemically ordered $Al_xGa_{1-x}N$ alloys: Spontaneous formation of natural quantum wells," Phys. Rev. B **71**, 035314 (2005).
[36]G. Stringfellow, "A critical appraisal of growth mechanisms in MOVPE," J. Cryst. Growth **68**, 111–122 (1984).
[37]G. B. Stringfellow, "Fundamentals of vapor phase epitaxial growth processes," AIP Conf. Proc. **916**, 48–68 (2007).
[38]M. Pristovsek, A. Kadir, and M. Kneissl, "Surface transitions during InGaN growth on GaN(0001) in metal–organic vapor phase epitaxy," Jpn. J. Appl. Phys. **52**, 08JB23 (2013).
[39]A. Munkholm, G. B. Stephenson, J. A. Eastman, C. Thompson, P. Fini, J. S. Speck, O. Auciello, P. H. Fuoss, and S. P. DenBaars, "Surface structure of GaN(0001) in the chemical vapor deposition environment," Phys. Rev. Lett. **83**, 741–744 (1999).
[40]C. G. Van de Walle and J. Neugebauer, "First-principles surface phase diagram for hydrogen on GaN surfaces," Phys. Rev. Lett. **88**, 066103 (2002).